HiSST: 3rd International Conference on
High-Speed Vehicle Science Technology
14 -19 April 2024, Busan, Korea

Progress in the development of a TPaSR model for the simulation of combustion in turbulent supersonic flows

Margot Pruvost[1], *Marc Ferrier*[2]
DMPE, ONERA, Université Paris Saclay, F-91123 Palaiseau, France
Arnaud Mura[3]
Ecole Nationale Supérieure de Mécanique et d'Aérotechnique, Futuroscope, France, 86961

Abstract

Simulating turbulent combustion in supersonic flows is a challenging yet essential task in designing scramjet combustors. In the high Reynolds number flows passing through the combustion chamber, mixing and chemical time scales have the same order of magnitude. Because of turbulence intermittency, dissipative structures are non-homogeneously distributed, leading to incomplete mixing of chemical species at the molecular level. In order to take into account this uneven distribution of the micro-mixed volumes in turbulent combustion simulations, Partially-Stirred-Reactor (PaSR)-like models have been developed. They assume that each computational cell is composed of a well-mixed region and its surroundings. However, considering a local model to describe the mixing process is a strong assumption since it does not take into account the whole history of micro-mixing. Furthermore, the chemical and mixing time scales are key parameters in these models and their estimation becomes challenging when dealing with complex configurations such as scramjet combustion chambers. In this paper, we introduce a new approach for the simulation of turbulent combustion and present its ongoing development. It is based on the PaSR concept together with a multi-fluid framework. In the computational domain, two fluids are considered: one relevant to the well-mixed volumes, and the other acting as their surroundings. Two sets of transport equations are considered to describe them. Within this Transported PaSR (TPaSR) framework, species micro-mixing and thermal diffusion are represented by source terms transferring mass and energy between the two fluids. In this study, expressions for mass and energy transfer are proposed and the model robustness is assessed on the NASA Langley Research Center supersonic coflowing burner. The model reproduces the regions within the mixing layer between fuel and oxidizer streams, and ensures mass transfer from one fluid to another at a higher rate in these regions.

Keywords: *CFD, Turbulence-chemistry interaction, PaSR, Supersonic combustion*

Nomenclature

Latin
e – Internal energy
E – Energy transfer term
h – Enthalpy
J – Mass diffusion flux
K – TPaSR constant
M – Mass transfer term
n – Unit vector
P – Pressure
q – Heat diffusion flux
s – Interface velocity
u – Flow velocity
Y – Chemical species mass fraction

Greek
γ – Fluid volume fraction
μ – Pressure relaxation parameter
ρ – Density

[1] *PhD student, Energetics Department, margot.pruvost@onera.fr*
[2] *Research Engineer, Energetics Department, marc.ferrier@onera.fr*
[3] *Senior Scientist, Fluids, Thermal Science and Combustion Department, PPRIME Institute UPR3346 CNRS, arnaud.mura@isae-ensma.fr*

σ – Interface area per unit volume
τ – Stress tensor
$\dot{\omega}$ – Production rate

Superscripts
π – Relative to fluid (π)

Subscripts
α – Relative to species α
i,j – Relative to direction i or j
s – Relative to the interface

1. Introduction

Scramjets and dual-mode ramjets are airbreathing engines currently developed to reach high flight Mach numbers relevant to hypersonic flow regimes. They offer significantly higher efficiencies compared to those of rocket engines when operating at low altitude [1,2]. Inside the combustion chamber of these engines, the airflow remains supersonic and features high Reynolds number values, creating a challenging environment for sustaining combustion. In this context, combustion stabilization is a sensitive matter and relies heavily on self-ignition processes since flow residence time scales and chemical time scales display similar orders of magnitude. Furthermore, the turbulent dissipative structures of the flow are unevenly distributed throughout the combustion chamber [3]. These structures represent regions where the micro-mixing of chemical species is the most intense, making them the most likely zones where combustion may develop.

To address the challenge of simulating such a non-homogeneous distribution of the reaction zones, turbulence-chemistry interaction (TCI) models such as the Partially Stirred Reactor (PaSR) models [4] or the eddy-dissipation concept (EDC) [5] have been developed. They are based on the splitting of each computational cell into two distinct regions. One of them represents the dissipative structures of the flow and is usually referred to as the (*) region. This area is the one where combustion can occur and is considered as a perfectly stirred reactor. The second region represents the surroundings, where chemical species are not mixed at the molecular level and cannot undergo chemical reactions. It is usually denoted as the (^{0}) region. Different variations of PaSR models have been derived from this concept in the literature [3,6]. However, most of them finally end up with a local, sometimes algebraic, model, which represents an important limitation. For instance, the thermochemical state of each region of the PaSR is determined assuming a local equilibrium between micro-mixing and species production, as given by Eq. 1:

$$\begin{cases} \overline{\rho}(Y_\alpha^* - Y_\alpha^0) = \tau_m \dot{\omega}_\alpha^*(T^*, Y_\alpha^*) \\ \overline{\rho}(h_s^* - h_s^0) = \tau_m \dot{\omega}_T^*(T^*, Y_\alpha^*) \end{cases} \quad (1)$$

with $\overline{\rho}$ the mean density, Y_α^* and Y_α^0 the (*) region and surroundings species mass fractions, $\dot{\omega}_\alpha^*$ the species production rate, $\dot{\omega}_T^*$ the heat release rate, h_s^* and h_s^0 the (*) region and surroundings sensible enthalpy and τ_m the mixing time scale.

The average or filtered species production rate is computed as follows:

$$\overline{\dot{\omega}_\alpha} = \gamma^* \dot{\omega}_\alpha^* \quad (2)$$

where γ^* is the (*) region volume fraction modeled with the following expression:

$$\gamma^* = (1 + \tau_m/\tau_c)^{-1} \quad (3)$$

This modeled (*) region volume fraction makes use of mixing (τ_m) and chemical (τ_c) time scales. In complex configurations such as those encountered in scramjet combustion chambers, where different combustion stabilization mechanisms are involved, it becomes difficult to define the values of these two characteristic times accurately. Furthermore, in order to better reproduce the mixing process and prevent the possible segregation of previously micro-mixed species, the PaSR model would benefit from the consideration of transport equations. To address these specific issues, we introduce a new PaSR model featuring transport equations for the two states (*) and (^{0}). This manuscript reports the ongoing development of the model.

2. Transported Partially Stirred Reactor Model (TPaSR)

2.1. General description

The new model, referred to as Transported Partially Stirred Reactor (TPaSR), has been inspired by both (i) the main hypothesis of the PaSR model, stating that each computational cell is split into two regions, and (ii) the two-fluid framework developed for two-phase flows. As a matter of fact, the TPaSR suggests that the well-mixed region (*) and the surrounding area (^{0}) of the PaSR model can be considered as two distinct fluids. With this in mind, chemical reactions can only happen in fluid (*). It is worth mentioning that the splitting of the domain into two fluids is just a mathematical and modelling construct, therefore, the interface between the fluids is not an actual one, and no chemical reaction or interfacial force do apply in this area. A sketch representing the operating principle of the TPaSR model is reported in Fig 1. It displays two streams of fuel and oxidizer entering a combustion chamber as fluid (^{0}) in blue, mixing together to generate fluid (*) in orange. Thanks to the retained multi-fluid approach, derived from the Baer-Nunziato theory [7], the model is no longer local and features transport equations for the quantities characterizing each fluid.

More specifically, the TPaSR model is implemented in the CFD code CEDRE developed at ONERA, in the framework of a new five-equation solver (MF5). When performing an asymptotical analysis on the Baer-Nunziato seven-equation theory, one can indeed establish that relaxing pressures and velocities of the two fluids to unique values, a five-equation system can be obtained [8]. The latter is implemented in the MF5 solver [9]. It assumes a unique pressure and velocity for both fluids but different temperatures and species mass fractions. With this approach, the temperature and composition of each fluid is no longer determined by a local equilibrium. As a matter of fact, due to numerical constraints, the equations solved in the MF5 solver include two different pressures, which are then relaxed to a unique value via a dedicated procedure. The system closure is achieved using a sixth transport equation on fluid (*) volume fraction. Conversely, the TPaSR model relies on two equations for the transport of mass, two equations for the transport of internal energy, one equation for the transport of momentum and one additional equation for the transport of fluid (*) volume fraction.

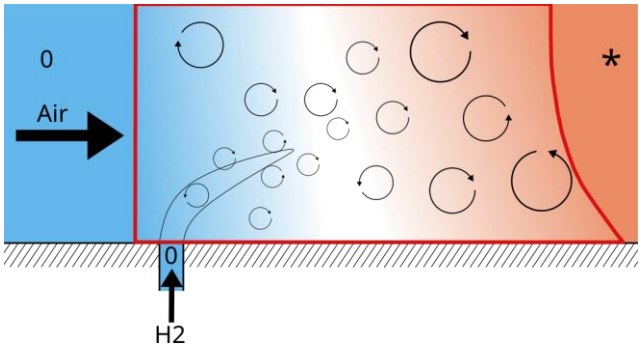

Fig 1. Combustion chamber featuring the two TPaSR fluids: fluid (^{0}) in blue and fluid (*) in orange.

In the MILES (Monotone Integrated Large Eddy Simulation) framework, i.e. without consideration of any sub-grid terms, the homogenized and filtered system of equations for the TPaSR model is given by Eq. 4:

$$\begin{cases} \frac{\partial}{\partial t}(\gamma^*\rho^*Y_\alpha^*) + \frac{\partial}{\partial x_j}(\gamma^*\rho^*Y_\alpha^*u_j) = -\frac{\partial}{\partial x_j}(\gamma^*J_{\alpha,j}^*) + \gamma^*\dot{\omega}_\alpha^* + M_{\alpha,0}^* \\ \frac{\partial}{\partial t}(\gamma^0\rho^0Y_\alpha^0) + \frac{\partial}{\partial x_j}(\gamma^0\rho^0Y_\alpha^0u_j) = -\frac{\partial}{\partial x_j}(\gamma^0J_{\alpha,j}^0) + M_{\alpha,*}^0 \\ \frac{\partial}{\partial t}(\rho u_i) + \frac{\partial}{\partial x_j}(\rho u_iu_j) = -\frac{\partial P}{\partial x_i} + \frac{\partial \tau_{ij}}{\partial x_j} \\ \frac{\partial}{\partial t}(\gamma^*\rho^*e^*) + \frac{\partial}{\partial x_j}(\gamma^*\rho^*e^*u_j) = -\frac{\partial}{\partial x_j}(\gamma^*q_j^*) - \gamma^*P^*\frac{\partial u_j}{\partial x_j} - \mu P^*(P^*-P^0) + \gamma^*\tau_{ij}^*\frac{\partial u_i}{\partial x_j} + E_0^* \\ \frac{\partial}{\partial t}(\gamma^0\rho^0e^0) + \frac{\partial}{\partial x_j}(\gamma^0\rho^0e^0u_j) = -\frac{\partial}{\partial x_j}(\gamma^0q_j^0) - \gamma^0P^0\frac{\partial u_j}{\partial x_j} - \mu P^0(P^0-P^*) + \gamma^0\tau_{ij}^0\frac{\partial u_i}{\partial x_j} + E_*^0 \\ \frac{\partial \gamma^*}{\partial t} + u_j\frac{\partial \gamma^*}{\partial x_j} = \mu(P^*-P^0) \end{cases} \quad (4)$$

with ρ, ρ^* and ρ^0 the mixing, fluid (*) and fluid (^{0}) density, Y_α^* and Y_α^0 the fluid (*) and fluid (^{0}) species mass fractions, γ^* and γ^0 the fluid (*) and fluid (^{0}) volume fractions, $J_{\alpha,j}^*$ and $J_{\alpha,j}^0$ the mass diffusion fluxes in fluid (*) and fluid (^{0}) in direction j, $\dot{\omega}_\alpha^*$ the species production rate in fluid (*), u the convection velocity, e^* and e^0 the fluid (*) and fluid (^{0}) internal energy, q_j^* and q_j^0 the fluid (*) and fluid (^{0}) heat diffusion fluxes in direction j, P^* and P^0 the pressure in fluid (*) and fluid (0), μ the pressure relaxation parameter, τ_{ij}^* and τ_{ij}^0 the fluid (*) and fluid (^{0}) viscous stress tensor, $M_{\alpha,0}^*$ and $M_{\alpha,*}^0$ the mass transfer terms between fluid (*) and fluid (^{0}) and E_0^* and E_*^0 the energy transfer terms between fluid (*) and fluid (^{0}).

In comparison with Eq. 3, the fluid volume fractions (γ^* and γ^0) are now determined as computational results. The modeling efforts are thus reported on the transfer source terms ($M_{\alpha,0}^*$ and E_0^*).

2.2. Focus on the mass transfer between fluids

Species micro-mixing is represented by mass transfer from fluid (^{0}) to fluid (*). Therefore, an expression must be established for the source term $M_{\alpha,0}^*$. First, two main hypotheses are taken into consideration:

i. Total mass conservation should be ensured: $M_{\alpha,0}^* = -M_{\alpha,*}^0 = M_\alpha$

ii. Molecular mixing can only progress: $M_\alpha \geq 0$

From the mass transport equations in a multi-fluid and multi-species framework (Eq. 4a and Eq. 4b), it can be demonstrated that the expression for the transfer source term is [10]

$$\mathrm{M}_\alpha^\pi = -\left(\rho^\pi Y_\alpha^\pi (u_i - s_i) - J_{\alpha,i}^\pi\right)\sigma_s n_i^\pi \tag{5}$$

with s_i the interface velocity, σ_s the interface area per unit volume and n_i^π the interface unit vector.

The mass transfer term in Eq. 5 consists in a convective and a diffusive part. As far as the diffusion contribution is concerned, it can be quite readily shown that, at the interface between the fluids, the sum of the corresponding fluxes over the whole set of chemical species is equal to zero. To satisfy this condition, and in a first modeling attempt, the diffusion fluxes ($J_{\alpha,i}^\pi$) are assumed to be zero. Let us recall that the interface is completely unknown. Hence, none of the quantities s_i, σ_s or n_i^π have a defined value. Since mass transfer should not depend, at least not directly, on the flow velocity, a hypothesis can be made on the form of s_i, as given by Eq. 6:

$$s_i = u_i - k(x, y, z, t) \tag{6}$$

with k a function of space and time.

In combination with Eq. 6, Eq. 5 can now be written as

$$\mathrm{M}_\alpha^\pi = -K(x, y, z, t)\rho^\pi Y_\alpha^\pi \tag{7}$$

In the framework of TPaSR, fluid (*) represents the portion of the flow in which the chemical species are mixed at molecular level in order to undergo chemical reactions. However, inside fluid (^{0}), molecular mixing is not achieved. Accordingly, the species micro-mixing is modeled by mass transfer from fluid (^{0}) to fluid (*). Thus, the expression for M_α^π should only depend on the quantities related to fluid (^{0}). Fluid (*) does not directly affect the mixing process. Furthermore, in order to decrease the transfer intensity when fluid (^{0}) disappears, we suggest to limit the transfer term by γ^0. Therefore, we propose a first model for M_α in Eq. 8:

$$M_\alpha = K(x, y, z, t)\gamma^0\rho^0 Y_\alpha^0 \tag{8}$$

The objective of the present work being to assess the model behavior on simple test-cases and to evaluate its robustness on a more complex configuration, K will be considered as constant.

Transferring mass from one fluid to another implies transferring the energy associated to this quantity. The MF5 solver includes internal energy transport equations. Therefore, it would seem reasonable to write the energy transfer term as the mass transfer term multiplied by fluid (^{0}) internal energy. However, adding a transfer term to the mass transport equations for each fluid implicitly affects fluid (*) volume fraction transport equation and leads to the addition of a supplementary pressure work term on the internal energy transport equations. The variation in internal energy caused by this additional term is balanced by making use of fluid (^{0}) enthalpy, instead of internal energy, in the energy

transfer term. Therefore, we suggest the following expression for the energy transfer term in the framework of the MF5 solver:

$$E^* = \sum_\alpha M_\alpha h^0 \tag{9}$$

with $E^0 = -E^*$.

This is of course only a line of reasoning. In order to properly demonstrate this expression, an asymptotical analysis on the Baer-Nunziato seven-equation system including transfer terms should be performed.

3. Reference cases

The TPaSR model is now assessed on different reference cases. First, zero- and one-dimensional computations are performed to investigate the model behavior and compare the numerical results to analytical solutions. The solver conservativity is also checked. Then, in order to examine the robustness of the model, as well as its phenomenological behavior, a three-dimensional case is performed. All of these preliminary tests are non-reactive. Indeed, the objective is to study the formation of fluid (*) in a first step.

3.1. Description of the zero- and one-dimensional cases

The first zero-dimensional test-case represents a closed domain filled with a mixture of ideal gas composed of two fluids (*) and (^{0}). Each fluid contains several chemical species. Initially, the gas is at rest and both fluids have the same temperature. Mass is transferred from fluid (^{0}) to fluid (*) via the transfer source terms, which represent micro-mixing induced by molecular diffusion. At first, the domain is full with fluid (^{0}), as the species are assumed to be unmixed at molecular level. As time passes and micro-mixing processes, the amount of fluid (*) increases. The initial conditions of the computation are reported in Table 1. In this case, the value of the constant in the mass transfer source term is $K = 10^5\ s^{-1}$.

Table 1. Initial conditions for the zero-dimensional test-case.

	$\mathbf{P}\ (\mathbf{Pa})$	$\mathbf{T}\ (\mathbf{K})$	$\mathbf{Y_{N_2}}(-)$	$\mathbf{Y_{O_2}}\ (-)$	$\mathbf{Y_{H_2O}}\ (-)$	$\mathbf{Y_{H_2}}(-)$	$\boldsymbol{\gamma}\ (-)$
Fluid (*)	60,000	500	0.7	0.3	0	0	0.05
Fluid (^{0})	60,000	500	0.56	0.23	0.17	0.04	0.95

The second test-case is one-dimensional and represents a constant section pipe of length 30 cm. In this pipe, a flow is entering from the left of the domain at constant velocity. It is composed of fluid (*) and fluid (^{0}), each one containing several chemical species. Both fluids have the same temperature. A transfer of mass from fluid (^{0}) to fluid (*) is taking place as a consequence of the transfer source terms. The inlet boundary conditions of the computation are reported in Table 2. In this case, the value of the constant in the mass transfer source term is $K = 10^4\ s^{-1}$.

Table 2. Inlet boundary conditions for the one-dimensional test-case.

	$\mathbf{P}\ (\mathbf{Pa})$	$\mathbf{T}\ (\mathbf{K})$	$\mathbf{u}\ (\mathbf{m/s})$	$\mathbf{Y_{N_2}}(-)$	$\mathbf{Y_{O_2}}\ (-)$	$\mathbf{Y_{H_2O}}\ (-)$	$\mathbf{Y_{H_2}}(-)$	$\boldsymbol{\gamma}\ (-)$
Fluid (*)	101,325	500	1150	0.56	0.23	0.17	0.04	0.05
Fluid (^{0})	101,325	500	1150	0.56	0.23	0.17	0.04	0.95

3.2. Description of the three-dimensional case

The chosen three-dimensional academic case is a supersonic burner developed at NASA Langley Research Center (LaRC). The experiment has initially been set up to examine the fundamental physical mechanisms underlying self-ignition of hydrogen-air mixtures and the stabilization of non-premixed combustion in supersonic flows, which are key parameters to understand the physical processes at play in a scramjet combustion chamber. This configuration has been experimentally investigated by Cheng et al. [11] and retained as a benchmark for many computational studies [3,12,13]. It consists in a coaxial injector featuring a sonic stream of hydrogen, surrounded by a Mach 2 coflow of hot vitiated

air. The experimental device is axisymmetric and is composed of a cylindrical central fuel injector of 2.36 mm in diameter and an annular convergent-divergent nozzle of 17.78 mm in outlet diameter. The setup is described with a schematic diagram in Fig 2. The nozzle accelerates the vitiated air stream, generated by the combustion of hydrogen into oxygen-enriched air in a primary chamber, up to Mach 2 (temperature 1250 K). The chamber is water cooled, as well as the fuel injector. The burner nominal operation conditions are reported in Table 3.

As far as the computation is concerned, the value of the constant in the mass transfer source term is $K = 10^5\ s^{-1}$. The main simulation is performed on a coarse mesh composed of 600,000 hexahedral cells, including the final part of the nozzle convergent. The purpose of using such a coarse mesh is to set up the model with relatively low-cost computations at first. A finer mesh, featuring 3,000,000 cells and prism layers along the walls has also been created in order to check the accuracy of the velocity profiles inside the computational domain. Since it is only possible to give static values of pressure and temperature as boundary conditions to the MF5 solver, the inlet boundary conditions are imposed in such a manner that the given stagnation conditions are recovered. These static values for the fuel and oxidizer streams are reported in Table 4. The imposed values are the same for fluid (*) and fluid (^{0}), apart from the volume fraction value, given on the final column of the table. It is worth mentioning that the quantities given in Table 4 are static values imposed at the entrance of the computational domain, whereas Table 3 displays some stagnation and static quantities at the nozzle exit. This explains the slight differences observed between the two datasets. Concerning the oxidizer static temperature given in Table 4, one can notice that the value used in the computation is far greater than the stagnation temperature given in Table 3. Indeed, as mentioned in reference [14], in order to recover the experimental temperature profile at the nozzle exit, a stagnation temperature of 2050 K, i.e. a static temperature of 2040 K, must be imposed on the inlet boundary condition.

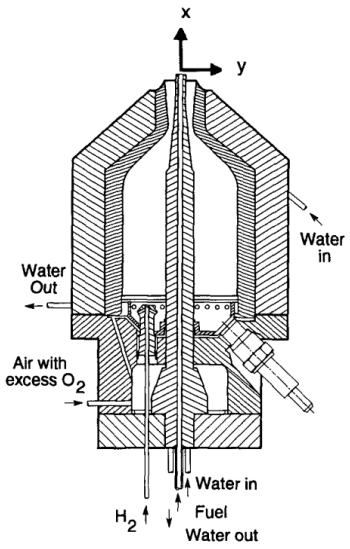

Fig 2. Schematic of the supersonic burner from reference [11].

Table 3. Supersonic burner nominal operation conditions [11].

Vitiated air conditions		**Fuel conditions**	
Stagnation conditions		**Stagnation conditions**	
Total pressure (Pa)	778,000 (±4%)	H_2 mass flow rate (kg/s)	0.000362 (±3%)
Total temperature (K)	1750		
Vitiated air mass flow rate (kg/s)	0.09633 (±2.2%)		
Exit conditions		**Exit conditions**	
Pressure (Pa)	107,000	Pressure (Pa)	112,000
Temperature (K)	1250	Temperature (K)	545
Mach (-)	2	Mach (-)	1
Velocity (m/s)	1420	Velocity (m/s)	1780
O_2 mass fraction (-)	0.245	H_2 mole fraction (-)	1
N_2 mass fraction (-)	0.580		
H_2O mass fraction (-)	0.175		

Table 4. Inlet boundary conditions for the computation with MF5 solver.

	$\mathbf{P}\ (\mathbf{Pa})$	$\mathbf{T}\ (\mathbf{K})$	$\mathbf{u}\ (\mathbf{m/s})$	$\mathbf{Y_{N_2}}(-)$	$\mathbf{Y_{O_2}}\ (-)$	$\mathbf{Y_{H_2O}}\ (-)$	$\mathbf{Y_{H_2}}(-)$	$\boldsymbol{\gamma^0}\ (-)$
Fuel	152,280	545	1220	0	0	0	1	0.999
Oxidizer	760,480	2040	165	0.580	0.245	0.175	0	0.999

4. Numerical aspects

The simulations are performed using the CFD code CEDRE [15,16] developed at ONERA. It solves the three-dimensional compressible and reactive Navier-Stokes equations on either structured or unstructured meshes and is based on a finite volume approach. In particular, the MF5 (Multi-Fluid 5 equations) solver is used with a specific procedure, relying on operator splitting, for time integration. Indeed, the MF5 equation system is split into two sub-systems, the first one being associated to convective and diffusive fluxes and the second one to pressure relaxation. In the code, a simple Lie splitting is performed. Therefore, the first sub-system is integrated using an explicit second order Runge-Kutta scheme and the transported quantities are updated. Then, the pressure relaxation operator is applied, which gives the transported quantities final value. It is worth noting that pressure relaxation is assumed infinitely fast, hence the second sub-system is not integrated in time using a regular scheme but a dedicated procedure [17,18]. The HLLC approximate Riemann solver, proposed by Toro et al. [19], is employed for inviscid fluxes and second-order spatial accuracy is achieved thanks to a multislope method [20]. Mass diffusion inside each fluid is neglected. Finally, in such simulations, high fluid volume fraction gradients may lead to some numerical issues in term of heat diffusion fluxes computation ($-\frac{\partial}{\partial x_j}\left(\gamma^{\pi} q_j^{\pi}\right)$ term in Eq. 4d and 4e). In order to overcome these difficulties, a dedicated scheme inspired by the work of Peluchon [21] and Petitpas [22] is used to compute the corresponding fluxes.

5. Results and discussion

5.1. Zero- and one-dimensional test-cases

In this section, the results obtained on the previous test-cases are reported. Let us remind that the aim of performing these test-cases is to check that the TPaSR model together with the MF5 solver behaves

properly on simple configurations featuring predictable results. First, the zero-dimensional case is studied. Fig 3 displays the change in volume fraction for each TPaSR fluid as a function of time. Analytical resolution of the problem is performed, and the results are compared to those obtained with CEDRE. As expected, fluid (^{0}) is occupying almost the whole volume at first. Then its volume fraction decreases as the one of fluid (*) increases. Therefore, species micro-mixing in fluid (^{0}) is well represented by mass transfer to fluid (*) and these numerical results are in very good agreement with the analytical ones.

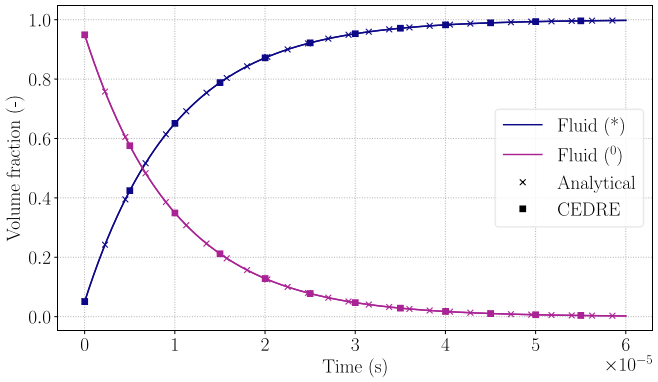

Fig 3. Time evolution of each fluid volume fraction.

It has been shown above in this document that the transfer source term on the internal energy transport equations should be: $E^* = \sum_\alpha M_\alpha h^0$. At first sight, this result seems a bit intriguing since it involves enthalpy and not internal energy. In order to support this expression, computations were performed using two different expressions for the energy transfer term: $E^* = \sum_\alpha M_\alpha e^0$ and $E^* = \sum_\alpha M_\alpha h^0$, where e^0 is the fluid (^{0}) internal energy and h^0 is its enthalpy. The results on the evolution of temperature are displayed in Fig 4. In such a computation, in which both fluids are initially at the same temperature without any heat released, the temperature of both fluids must remain constant and equal to their initial common value. Yet, it is shown on the left part of Fig 4 that when using internal energy instead of enthalpy in the transfer term, the temperature of fluid (^{0}) rises sharply up to almost 4050 K, which lacks coherence. On the opposite, on the right-hand side of the figure, the temperature of both fluids remains at a constant value of 500 K, showing the need of using enthalpy in the energy transfer term and confirming the choice made in section 2.2.

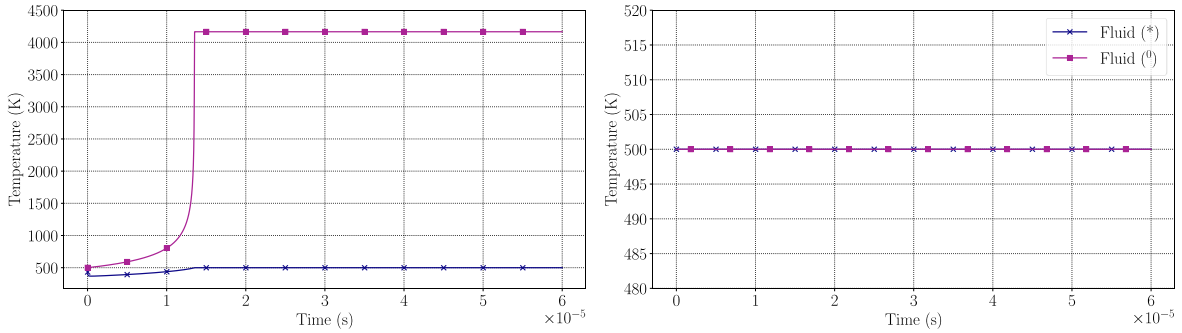

Fig 4. Time evolution of each fluid temperature. Left: $E^* = \sum_\alpha M_\alpha e^0$, right: $E^* = \sum_\alpha M_\alpha h^0$.

Continuing with the mono-dimensional case, the first objective of this computation is to check the MF5 solver conservativity when performing mass transfer between the two fluids. To this purpose, the sum over all the chemical species of the incoming and outgoing mass fluxes is computed. Its temporal evolution is displayed in Fig 5. It reveals an unsteady behavior until the initial state is replaced by the imposed inlet boundary condition. Then, at around 0.3 ms, steady-state is reached and the sum of the mass fluxes becomes null. The conservativity of the MF5 solver in presence of mass transfer between fluids is confirmed.

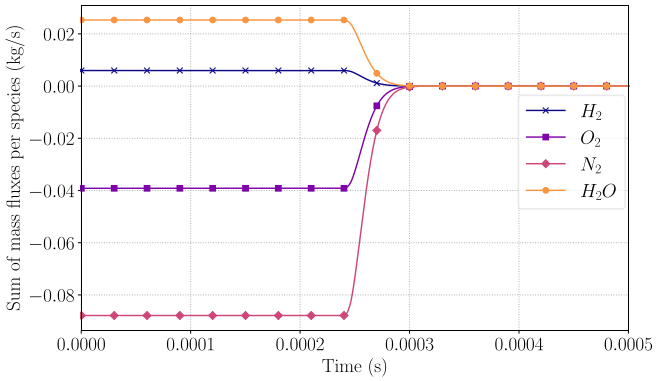

Fig 5. Time evolution of the sum of the incoming and outgoing mass fluxes.

The second goal relevant to this one-dimensional case is, as for the zero-dimensional case, to check the model behavior and compare the results given by CEDRE with a reference solution. In particular, an analytical solution to this problem can be found, for steady-state conditions, regarding the evolution of the fluids volume fractions along the x-axis. Fig 6 shows the change in volume fraction for each TPaSR fluid along the domain. It compares the analytical solution to the results given by CEDRE using the TPaSR model. Both of them are in excellent agreement.

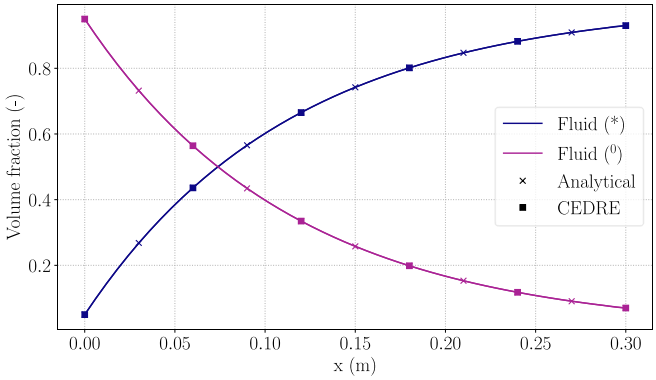

Fig 6. Spatial evolution of each fluid volume fraction at steady-state.

5.2. Three-dimensional case: supersonic burner

Prior to using the TPaSR model, computations were performed on the meshes containing 600,000 and 3,000,000 cells with the MF5 solver. The aim is to assess the choice of inlet boundary conditions. To this purpose, the axial velocity profiles on four different sections downstream of the injector have been plotted in Fig 7. A comparison is made between MF5 results obtained on the two different meshes, the numerical results obtained by Moule et al. [3] and experimental data [23]. The different sections are chosen at distances of 10.8, 21.5, 32.3, and 43.1 diameters from the nozzle exit. At the first position downstream of the injector, an important difference of around 200 m/s between experimental and numerical results can be observed. The lower velocities measured in the experiment are due to the fact that seeding particles do not perfectly follow the gas flow when experiencing strong accelerations, as documented in reference [11]. Moreover, again in the first section, the profile obtained with the MF5 solver on the coarsest mesh displays a velocity peak on the center axis, whereas experiments and reference numerical results show a velocity decrease in this area. This difference is due to the poor level of resolution of the mesh and the right tendency is recovered when performing the MF5 computation on the finer mesh. Provided that a 3,000,000-cell mesh is still quite coarse to study such a configuration, the results lead us to believe that refining even more the mesh would allow to recover satisfactorily the centerline velocity drop. In this respect, it must be recalled that, the mesh used by Moule et al. [3] features 31,000,000 cells. Moving on to the other sections where the axial velocity was measured, the profiles obtained with the MF5 solver are quite similar to the reference data, especially in terms of maximum value. It is however worth noticing that the jet development is better reproduced by the computation using the 3,000,000-cell mesh. In conclusion, the velocity profiles obtained on the

600,000-cell mesh do not perfectly match the experimental and reference numerical data, but it is considered to be sufficient for proceeding with a preliminary analysis of the TPaSR model. Using such a mesh indeed gives the opportunity to perform reduced-cost computations for the setup of the model.

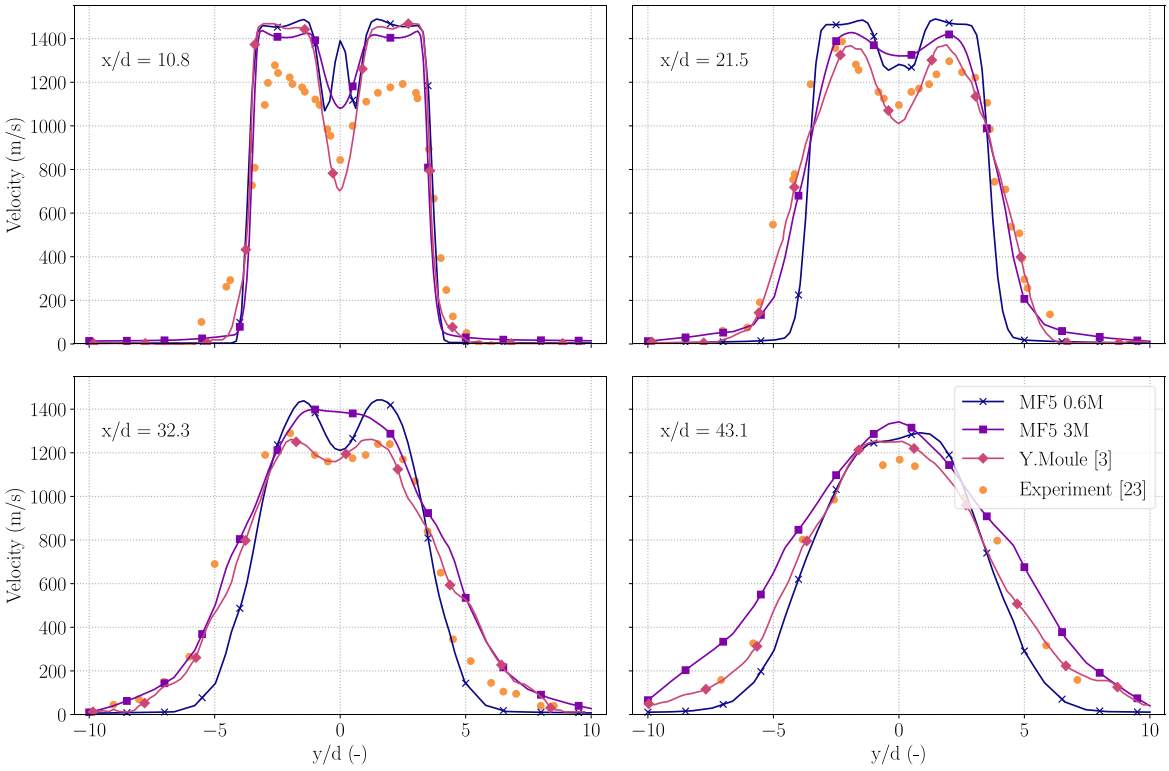

Fig 7. Mean axial velocity profiles at four sections downstream of the injector (x/d = 10.8, x/d = 21.5, x/d = 32.3 and x/d = 43.1). Comparison of the MF5 solver results on the two different meshes with numerical [3] and experimental data [23].

Thus, a TPaSR computation is carried out on the three-dimensional burner geometry and some unsteady results are presented hereafter. For instance, Fig 8 shows fluid (*) volume fraction in the mid-plane section of the configuration. Indeed, fluid (*) formation is observed in the mixing layer between the fuel and oxidizer streams, that is to say the area where combustion might occur. Moreover, significant variations in the fluids volume fractions can be noticed from one cell to another in the area surrounding fluid (*) formation. As mentioned earlier, the dedicated numerical scheme used for the computation of heat diffusion fluxes ensures the robustness of the simulation. These first results reveal that the TPaSR model behaves properly regarding the production of fluid (*). The next steps will consist in (i) adjusting parameter K, on the basis of turbulence characteristic frequencies, so as to be more representative of the physics, in order to be able to perform reactive simulations and (ii) comparing, in a quantitative way, the TPaSR results to the experimental and computational data previously documented in the literature.

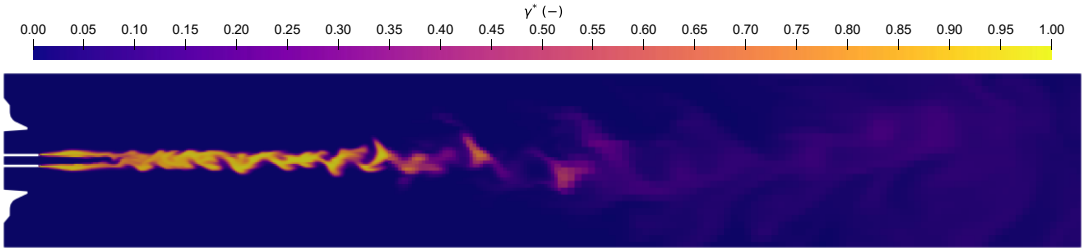

Fig 8. Volume fraction of fluid (*) field on the mid-plane section.

6. Conclusion

In this paper, we introduced a new model referred to as TPaSR, based on both the PaSR model and a multi-fluid approach, for the simulation of turbulent combustion in supersonic flows. The model has been implemented in the CFD code CEDRE [15,16] developed at ONERA, in the framework of a new multi-fluid solver (MF5) [9]. Compared to the PaSR model, TPaSR does not need to estimate a value for the mixing and chemical characteristic times, which are difficult to determine in complex configurations such as scramjet combustion chambers. The modeling effort is reported on mass and energy transfer source terms between fluids. An expression has been suggested for both of these terms and the model behavior, as well as the MF5 solver conservativity, have been tested on several non-reactive cases. First, zero- and one-dimensional computations were performed and showed a very good level of agreement between the computational model results and the analytical solutions, as well as a satisfactory behavior of the MF5 solver in terms of conservativity in the presence of mass and energy transfers between the fluids. The model and solver assessment is pursued on a three-dimensional supersonic burner configuration. Consistent results have been observed, with the production of fluid (*) in areas of interest.

The next step of the work will be concerned with the specification of the characteristic frequency K that drives the mass transfer term between the two fluids. The consideration of heat diffusion in the energy transfer term will also be studied. Then, reactive computations on a refined mesh will be performed and the results compared to those available in the literature.

Acknowledgments

The present work was conducted within the framework of a Ph.D. grant co-funded by AID Ministry of Defense and ONERA. Additionally, the authors would like to thank Clément Le Touze, Alexia De Brauer and Nicolas Rutard for their numerous developments on the MF5 solver, as well as Dominique Scherrer for the fruitful conversations on the TPaSR model.

References

1. M. Smart, "Scramjets," *The Aeronautical Journal*, no. 111, pp. 605-620, 2007.
2. C. Segal, *The Scramjet Engine - Processes and Characteristics*, Cambridge University Press, 2009.
3. Y. Moule, V. Sabelnikov, and A. Mura, "Highly resolved numerical simulation of combustion in supersonic hydrogen-air coflowing jets," *Combustion and Flame*, vol. 161, pp. 2647-2668, 2014.
4. M. Berglund, E. Fedina, C. Fureby, J. Tegnér, and V. Sabelnikov, "Finite rate chemistry Large-Eddy Simulation of self-ignition in a supersonic combustion ramjet," *AIAA Journal*, no. 48, 2010.
5. B.F. Magnussen, "On the structure of turbulence and a generalized eddy dissipation concept for chemical reaction in turbulent flow," *AIAA*, 1981.
6. V. Sabelnikov and C. Fureby, "LES combustion modelling for high Re flames using a multi-phase analogy," *Combustion and Flame*, no. 160, pp. 83-96, 2013.
7. M.R. Baer and J.W. Nunziato, "A two-phase mixture theory for the deflagration-to-detonation transition (DDT) in reactive granular materirals," *International Journal of Multiphase Flow*, no. 12, pp. 861-889, 1986.
8. A. Murrone and H. Guillard, "A five equation reduced model for compressible two phase flow problems," *Journal of Computational Physics*, no. 202, pp. 664-698, 2005.
9. C. Le Touze and A. Murrone, "Développement d'un modèle multifluide à 5 équations dans CEDRE (Development of a 5-equation multifluid model in CEDRE)," ONERA - Multi-Physics for Energetics Department, Technical report 2020.
10. R. Borghi and F. Anselmet, *Turbulent Multiphase Flows with Heat and Mass Transfer*, ISTE Ltd, 2014.

11. T. S. Cheng, J.A. Wehrmeyer, R.W. Pitz, O. Jarrett, and G.B. Northam, "Raman measurement of mixing and finite-rate chemistry in a supersonic hydrogen-air diffusion flame," *Combustion and Flame*, no. 99, pp. 157-173, 1994.
12. T. Bridel-Bertomeu and P. Boivin, "Explicit chemical timescale as a substiture for tabulated chemistry in a H2-O2 turbulent flame simulation," *Combustion Science and Technology*, no. 187, pp. 739-746, 2015.
13. L. Gomet, V. Robin, and A. Mura, "Influence of Residence and scalar mixing time scales in non-premixed combustion in supersonic turbulent flows," *Combustion Science and Technology*, no. 184, pp. 1471-1501, 2012.
14. Y. Moule, "Modélisation et simulation de la combustion dans les écoulements rapides. Application aux superstatoréacteurs (Modeling and simulation of combustion in high velocity flows. Application to scramjets)," PhD thseis 2013.
15. A. Refloch et al., "CEDRE Software," *Aerospace Lab*, no. 2, pp. 1-10, 2011.
16. D. Scherrer et al., "Recent CEDRE Applications," *Aerospace Lab*, no. 2, pp. 1-28, 2011.
17. G.H. Miller and E.G. Puckett, "A high-order Godunov method for multiple condensed phases," *Journal of Computational Physics*, no. 128, pp. 134-164, 1996.
18. R. Saurel, F. Petitpas, and R.A. Berry, "Simple and efficient relaxation methods for interfaces separating compressible fluids, cavitating flows and shocks in multiphase mixtures," *Journal of Computational Physics*, no. 228, pp. 1678-1712, 2009.
19. E.F. Toro, M. Spruce, and W. Spears, "Restoration of the Contact Surface in the HLL-Riemann solver," *Shock Waves*, no. 4, pp. 25-34, 1994.
20. C. Le Touze and A., Guillard, H. Murrone, "Multislope MUSCL method for general unstructured meshes," *Journal of Computational Physics*, no. 284, pp. 389-418, 2015.
21. S. Peluchon, G. Gallice, and L. Mieussens, "Developement of numerical methods to simulate the melting of a thermal protection system," *Journal of Computational Physics*, no. 448, 2022.
22. F. Petitpas and S. Le Martelot, "A discrete method to treat heat conduction in compressible two-phase flows," *Computational Thermal Sciences: An International Journal*, vol. 3, no. 6, 2014.
23. O. Jarrett et al., "Measurements of temperature, density, and velocity in supersonic reacting flow for CFD code validation," *25th JANNAF Combustion Meeting*, vol. 1, pp. 357-374, 1988.